Soil development on basic and ultrabasic rocks in cold environments of Russia traced by mineralogical composition and pore space characteristics

Sofia N. Lessovaia [a,d,*], Stefan Dultz [b], Michael Plötze [c], Natalia Andreeva [d], Yury Polekhovsky [a], Alexey Filimonov [d], Olesya Momotova [e]

[a] *St. Petersburg State University, Institute of Earth Science, V.O., 10 line, 33, St. Petersburg 199178, Russia*
[b] *Leibniz Universität Hannover, Institute of Soil Science, Herrenhäuser Str. 2, D-30419 Hannover, Germany*
[c] *ETH Zurich, Institute for Geotechnical Engineering, CH-8093 Zurich, Switzerland*
[d] *St. Petersburg State Polytechnical University, 29 Politekhnicheskaya, 195251 St. Petersburg, Russia*
[e] *Belgorod State University, ul. Pobedy 85, Belgorod, Russia*

ARTICLE INFO

ABSTRACT

Recent soils from basic (amphibolite and meta-gabbro amphibolite) and ultrabasic (serpentinous dunite) rocks formed in cold and humid climates of Northern Eurasia (Russia) were studied to detail the characterization of soils and rocks with special attention to the interdependence of porosity system and rock mineralogy. The study plots were located in taiga and tundra zones of East Fennoscandia and the Polar Ural Mountains. A variety of methods was used including optical microscopy, X-ray diffraction and Rietveld analysis, and three supplemental methods for the determination of pore space characteristics in rocks: (i) mercury intrusion porosimetry, (ii) a modification of this method using the intrusion of a molten alloy (Wood's metal), and (iii) scanning atomic-force microscopy. The results illustrate that the specification of the porosity system is a significant factor in tracing the clay mineralogy in soils formed from hard rocks. Ultrabasic rock is the most sensitive to weathering, as determined by (i) the high value of small pores, especially those with a radius of < 10 nm, (ii) the elongated form of the pores and surface roughness, and (iii) zones with an accumulation of phyllosilicates in regions with higher porosity causing the formation of soil enriched by clay minerals.

Despite the presence of low proportions of phyllosilicates in both types of basic rocks, only soil from meta-gabbro amphibolite is enriched by clay minerals and is most probably affected by small pores (< 10 nm). The absence of phyllosilicate accumulation along the pores and the predominantly empty space inside the pores indicates the limitation of potential sources of phyllosilicates for developing soils from meta-gabbro amphibolite. Insignificant phyllosilicate accumulation in shallow soil from amphibolite, in which the fine size fractions are mostly the result of rock disintegration, is supposedly due to a particularly narrow pore size distribution with a predominance of pores between 100 and 1000 nm.

1. Introduction

In cold environments, freezing–thawing cycles significantly affect pedogenesis, especially in the case of soil formation from hard rocks. Rock disintegration results in an increase in surface area, which is sensitive to chemical weathering (Arnaud and Whiteside, 1963; Allen, 2002), element release and the appearance of secondary minerals (Velde and Meunier, 2008). Adopting the approach of Velde and Meunier (2008) the interactions between primary minerals and solutions often take place within confined or semi-confined microenvironments such as pores rather than in a bulk solution. This approach is particularly relevant to studies of the early stages of clay mineral development on weathering and the environment in which this particular study takes place: extreme cold, where weathering occurs slowly.

The transformation of minerals in the soil environment has even been reported for extremely cold conditions, such as in the arctic tundra of Northern Alaska (Gelisols) (Borden et al., 2010), the ice-free areas of King George Island, Antarctica (Cryosols) (Simas et al., 2006), and the taiga zone from the Central Yakutia plain with its extra-continental climate (Cryosols) (Lessovaia et al., 2013). Nevertheless, the number of observations of pedogenesis from hard rocks traced by mineralogical composition and pore space characteristics is still low. Data from tundra and taiga zones of Eurasia, especially mineralogy and micromorphology, show that clay minerals in the soils from hard rocks are

* Corresponding author at: St. Petersburg State University, Institute of Earth Science, V.O., 10 line, 33, St. Petersburg 199178, Russia. Tel.: +7 812 323 39 13.
E-mail address: sofia.lessovaia@mail.ru (S.N. Lessovaia).

Fig. 1. Location of the key plots in East Fennoscandia (1) and the Polar Urals (2).

mostly inherited; they are not detected in the soil if they are absent in the hard rock (Sedov et al., 1992; Chernyakhovskii, 1994). However, other investigations have shown that considerable amounts of smectite, which is absent in the rock, appear in the fine earth derived from that rock (ultrabasic type) and soils (Lessovaia et al., 2012). Based on these divergent findings, the aim of this study is to produce a detailed characterization of soils from basic and ultrabasic rocks formed in cold climates in Northern Eurasia (Russia) with special attention to the interdependence of the porosity system and rock mineralogy.

2. Materials

Holocene soils from basic and ultrabasic rocks formed in cold and humid climates were studied. The first study plot was located in the taiga zone of East Fennoscandia (GPS coordinates: 67°32′ 65″ N and 33°46′ 08″ E) (Fig. 1). The "dot" (intermittent) distributed residual ridges (selgas) of amphibolite are surrounded by the acidic moraine material from the last glaciation. Local accumulation of fine earth was observed only in small cavities in the rock. Very shallow soils, classified as Lithic Leptosols according to WRB (2006), have been developing at this site. The second study plot was situated in the taiga zone of the Polar Urals that is a part of the Ural Mountains in the Arctic Circle

(GPS coordinates: 66°48′ 31.2″N and 65°46′ 20.1″E). A more mature profile of Epileptic Entic Podzol (Pit Y-05-07) on a flat outcrop of meta-gabbro amphibolite is described here. The third study plot was located on the flat summit in the mountainous tundra of the Polar Urals (the Rai-Iz massif that is made up of ultrabasic rock) at an altitude of 664 m (GPS coordinates: 66°52′ 03.3″ N and 65°19′ 33.6″′ E), and permafrost began at a depth of 30 cm. Due to intensive gleization, the fine earth that accumulated on the blocks of serpentinous dunite had a bright color. The soil is classified as Haplic Cryosol (Reductaquic) (Pit Y-02-07).

3. Methods

The fine soil (the <1 mm fraction) was separated by dry sieving. Bulk chemical composition of the <1 mm soil fraction and rock samples was determined by X-ray fluorescence analysis (Tefa-611, EG&G Instruments Ortec). The proportion of Fe^{2+} in the rock samples was determined by colorimetric wet-chemical analysis (Schuessler et al., 2008). Soluble Fe forms in the <1 mm fraction were obtained through extractions with dithionite (Mehra and Jackson, 1958) and oxalate (Fe and Al) (Jackson et al., 1986). pH-values were measured potentiometrically in H_2O with a soil:water ratio of 1:2.5. C-content was determined by wet combustion using the Tyurin (1931) method. For the upper horizons that contained fair amounts of organic matter, loss on ignition was determined. The content of the <1 μm fraction of the soil was determined by sedimentation with the pipette method.

Mineral association of the rock samples from the lithic contact were studied in thin sections by optical microscopy (Zeiss Axioplan 2 and Polam P-312 microscopes). Three supplemental methods for the determination of the pore space characteristics were applied: (i) mercury intrusion porosimetry (MIP) for the quantification of total porosity and pore size distribution, (ii) a modification of this method using the intrusion of a molten alloy (Wood's metal) and subsequent electron microscopy on the polished sections to determine the micro-morphology of the connective pores and to detect closed pores, and (iii) scanning atomic-force microscopy (AFM) to obtain quantitative pore dimension data.

MIP was carried out with a combined instrument (Pascal 140 + 440, POROTEC) for measuring macro- and mesopores with radii in the range of 58000–1.8 nm. The instrument only determines the percentage of open (connective) pores that are Hg-accessible. The measurements were conducted by incrementally increasing the pressure up to 400 MPa. The pore size distribution was determined according to the

Table 1
pH, C-content, share of <1 μm fraction, chemical composition and dithionite and oxalate soluble Fe and Al of the studied soils.

Horizon, depth (cm)	pH H₂O	C/LI (%)	<1 μm (%)	Chemical composition of soil, the <1 mm fraction (% in ignited sample)									Fe₂O₃d	Fe₂O₃o	Al₂O₃o	Fe²⁺ (wt.%)
				SiO₂	Al₂O₃	Fe₂O₃	CaO	MgO	K₂O	Na₂O	MnO	TiO₂		(%)		
Lithic Leptosol on amphibolite, Pit X-05-3																
A 0–2	4.4	32.0/44.8	–	61.44	11.30	10.32	8.43	1.62	0.67	1.40	0.19	2.93	1.09	0.74	0.41	–
Bw 2–6	4.5	7.6	9.7	61.44	11.96	11.39	8.01	2.17	0.30	1.07	0.14	2.75	1.07	0.48	0.26	–
R	–	–	–	54.76	12.04	17.23	10.57	2.87	0.12	0.86	0.18	1.26	–	–	–	–
Epileptic Entic Podzols on meta-gabbro amphibolite, Pit Y-05-07																
O2 0–3	4.5	26.3/71.2	–	70.16	11.49	6.95	3.97	3.03	1.24	1.56	0.11	0.89	0.88	0.38	0.31	–
Bw 3–5	4.4	3.7	15.3	73.44	11.43	6.82	2.05	2.39	0.98	1.58	0.08	0.98	1.95	0.60	0.59	5.06
Bhs 5–10	4.9	2.5	16.7	71.03	12.60	7.73	2.20	2.77	0.96	1.56	0.08	0.93	2.17	0.46	0.96	3.92
Bs 10–24	5.6	1.0	9.7	67.83	14.25	7.69	2.60	3.74	1.10	1.56	0.10	0.80	1.65	0.50	1.48	–
BC 24–30	6.1	0.6	7.7	66.50	14.36	7.70	2.99	4.48	1.11	1.88	0.12	0.76	1.26	0.39	1.32	5.05
R	–	–	–	55.87	16.27	10.44	8.06	5.64	0.39	2.51	0.19	0.40	–	–	–	–
Haplic Cryosols (Reductaquic) on serpentinous dunite, Pit Y-02-07																
Ah 0–4	7.2	4.5/16.3	7.8	54.59	5.05	10.62	1.35	25.88	0.75	0.63	0.23	0.38	2.68	1.79	0.08	6.22
Bg 4–15	7.0	4.7	6.8	56.00	5.70	11.25	1.43	22.57	0.86	0.96	0.20	0.42	4.05	2.57	0.11	5.85
Bgf 15–30	8.0	1.9	17.4	65.92	8.66	7.10	1.44	13.23	1.35	1.20	0.07	0.65	1.53	0.66	0.11	4.37
R	–	–	–	44.52	0.72	12.87	0.85	40.34	0.10	<0.05	0.21	0.02	–	–	–	–

Abbreviations and notes: C — total carbon; LI — loss on ignition; <1 μm — content of particle size <1 μm in the <1 mm fraction; '–' — no data available; d — dithionite and o — oxalate extractable Fe₂O₃ and Al₂O₃; Fe²⁺ (wt.%) determined by colorimetric wet-chemical analysis, R — rock samples from lithic contact.

Washburn equation, which yields a relationship between pressure and pore size (Washburn, 1921):

$$r = -\frac{2\gamma \cos\Theta}{p}$$

where r = pore radius, p = pressure, γ = surface tension of mercury = 0.48 N/m, and Θ = wetting angle of mercury (135°).

The advantage of the intrusion of the molten alloy, 'Wood's metal', for pore structure studies is the determination of the local porosity where the physical distribution and the connectivity of the pores can be examined (Lloyd et al., 2009). In addition, this method allows for an improved description of the pore textural characteristics and a visualization of the secondary minerals in the pore space. The eutectic alloy of 50% Bi, 25% Pb, 12.5% Sn, and 12.5% Cd by weight has a melting point at 78 °C. Sections of the rocks were intruded with the molten alloy at 100 °C with a pressure of 55 MPa in evacuated samples (Dultz et al., 2006; Kaufmann, 2009). Based on the Washburn equation (see description of MIP), intruding the alloy at a pressure of 55 MPa corresponds to a pore diameter of ~20 nm, using a surface tension of 0.48 N/m and a contact angle of 130° (Darot and Reuschle, 1999). After solidification of the alloy, polished sections were prepared, sputtered with Au and the invaded connective pore system was examined in back-scattered electron images (FEI, QUANTA 200).

The surface topography of the rocks was studied using the AFM technique (Nano-DST atomic-force microscope Nanopacific Technology, CA) on scans of 50×50 μm and 10×10 μm sections. Standard statistical parameters (mean value of the height irregularities and root mean square (RMS) value of the height irregularity) were calculated for the 50×50 μm image using Gwyddion software (GNU General Public License). The total projected area of the pores was evaluated by a watershed algorithm (Klapetek et al., 2003), which is dependent on the
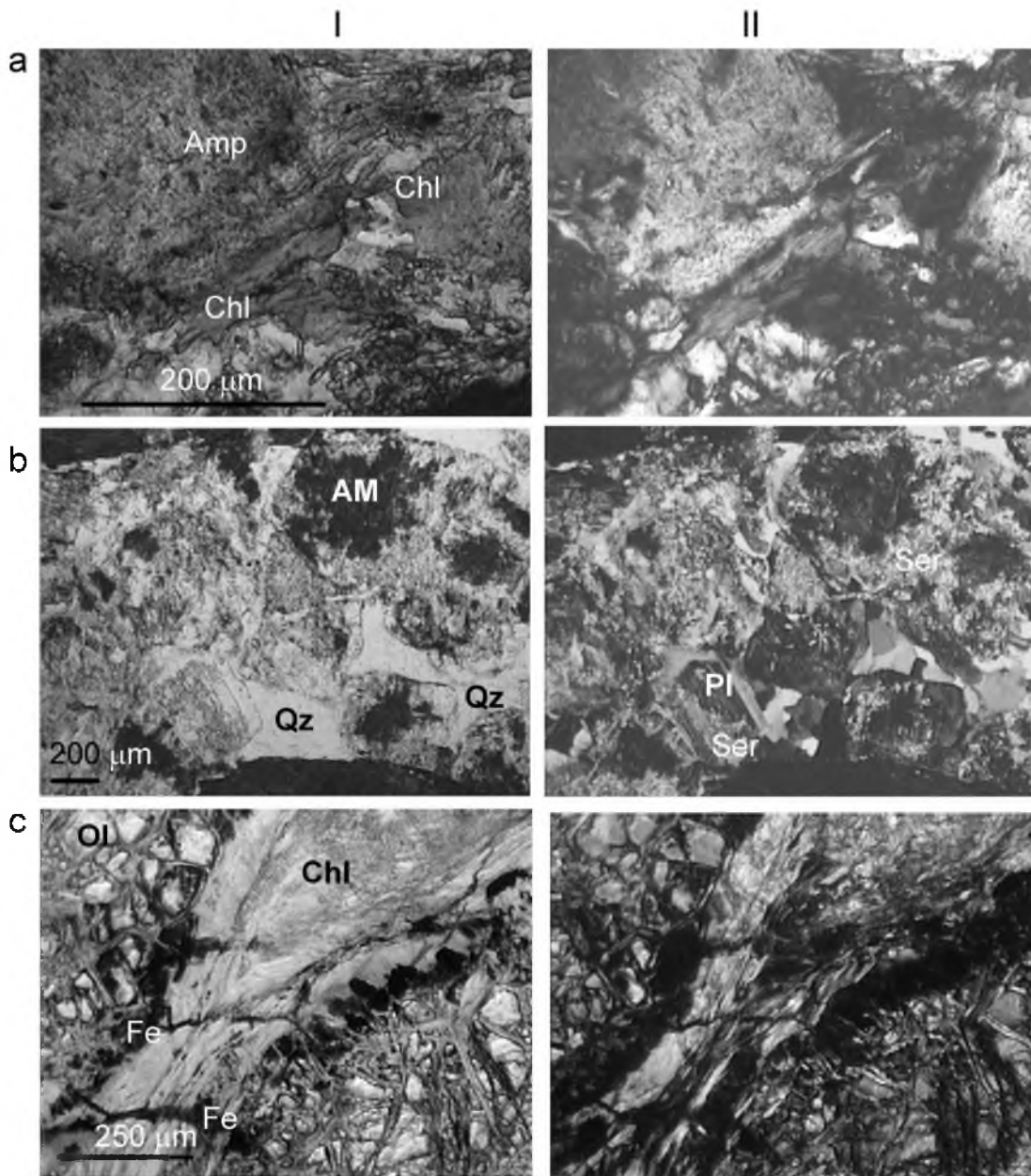
Fig. 2. Micromorphology of the rock samples: replacement of amphiboles by chlorite in amphibolite from Lithic Leptosol (a); mineral association of meta-gabbro amphibolite from Epileptic Entic Podzol (b); and broken grains of olivine and formation of Fe-oxides in micro-cracks of serpentinous dunite from Haplic Cryosols (Reductaquic) (c). Observations on thin sections at (I) plain polars and (II) crossed nicols. Symbols for the minerals originate from Whitney and Evans (2010) and are modified to some part: Amp — amphibole, Chl — chlorite, Ol — olivine, Pl — plagioclase (group name), Ser — sericite, Qz — quartz, and Fe — Fe-oxides, and AM — weakly anisotropic mass.

placement of the scan caused by sample topography. The most typical areas were scanned. It was assumed that (i) the microstructure is mostly self-affine (self-similarity, which is meant that the object is exactly or approximately similar to a part of itself) and (ii) the fractal dimension is the local Hausdorff–Besicovitch dimension, D. The self-affine properties of the microstructure were also evaluated by fractal analysis using two methods: (i) cube counting and (ii) binary decomposition of the image intensity field.

The quantitative mineralogical composition of the rock samples was determined by X-ray diffraction and Rietveld analysis. A representative aliquot of approximately 1 g of crushed rock material was milled in ethanol to a grain size of less than 20 μm with a McCrone micronizing mill (McCrone Scientific). Adding zincite as an inner standard (final content 20 wt.%) allows for the quantification of amorphous content. X-ray diffraction measurements were made using a Bragg–Brentano diffractometer (Bruker AXS D8 advance using CoKα radiation) with an automatic divergence and anti-scattering slit, primary and secondary 4° soller slits, and a Sol-X solid state detector. The powdered samples were step-scanned at room temperature from 2 to 80° 2Θ (step width 0.02° 2Θ, counting time 4 s). The qualitative phase composition was determined with the DIFFRACplus software (BRUKER AXS). On the basis of the peak position and their relative intensity, the mineral phases were identified in comparison to the ICDD database. The quantitative composition was calculated by Rietveld analysis of the XRD pattern (Rietveld program AutoQuan, GE SEIFERT) (Bergmann et al., 1998; Bergmann and Kleeberg, 1998; Bish and Plötze, 2011).

4. Results

4.1. Soil properties

Both soil profiles from the basic rocks are acidic. Pronounced acidification of the upper horizons (O2–Bw) in mature Epileptic Entic Podzol is identified. In Pit Y-02-07, from ultrabasic rock, the pH value is neutral in the upper horizon (0–15 cm) and slightly alkaline in the bottom, which indicates that the possibility of soil alkalinity development induced not by calcareous but by ultrabasic material (Table 1). Despite the predominance of the coarse-grained fractions in all profiles, the proportion of <1 μm fraction, even in the shallow profile (Pit X-05-3), is ~10%, which indicates a sensitivity to weathering and alteration of the parent materials. In spite of the shallow depth of Pit X-05-3 and the basic nature of amphibolite being confirmed by bulk chemical composition, the SiO_2 content in Lithic Leptosol is higher than it should be in the basic material. However, specific chemical composition of the rock as well as the marked proportion of CaO and TiO_2 and, especially, Fe_2O_3 is pronounced in the profile. Low proportions of soluble Fe, mostly represented by the oxalate extractable form, and Al, indicate weak development of pedogenesis in Lithic Leptosol.

In Epileptic Entic Podzol, as well as in meta-gabbro amphibolite, the proportion of SiO_2 is higher than it should be in the basic material. In the profile, the upper horizons, with the exception of the O2-horizon, are enriched by dithionite extractable Fe, indicating stronger weathering intensity than in Lithic Leptosol. Additionally, the lower proportion of Fe^{2+}, which is connected mostly with inherited silicates, in the Bhs horizon is linked with high concentrations of dithionite extractable Fe due to the oxidation of released Fe. The formation of well-crystallized, pedogenic Fe-oxides is confirmed by a low amount of oxalate extractable forms. The higher proportion of soluble Al in the Bs–BC horizons is most probably a result of residual accumulation of more stable material in the upper part due to podzolization.

In Haplic Cryosol (Reductaquic), the proportions of SiO_2 and Al_2O_3, which are significantly higher than in serpentinous dunite, indicate the possible influence of allochthonous material. The latter could be confirmed by an increase in the proportion of Fe^{2+} towards the upper horizon that would indicate that the allochthonous substrate is less weathered than the ultrabasic one. Nevertheless, high contents of total

MgO and soluble Fe reflect the predominance of ultrabasic substrate as deduced from the SiO_2 content and the extremely low proportion of Al_2O_3, which indicate the presence of silicates enriched by Mg and poor in Al. Pedogenesis caused the marked eluvial–illuvial distribution of the Fe-extractable forms.

4.2. Rock characteristics

4.2.1. Petrography and mineralogy of rocks (thin section and XRD data)

The association of the minerals detected by X-ray diffraction completes the results obtained from the thin sections. Amphiboles (mainly actinolite and hornblende) are predominant (38.4 wt.%) in amphibolite (Pit X-05-3) (Fig. 2, Table 2). Amphiboles are often replaced by epidote (26.7 wt.%) and chlorite (7.0 wt.%). Plagioclase (~10 wt.%) mostly shows saussuritization (replacement by several minerals). The high amount of the X-ray amorphous phase (14.3 wt.%), which is also visible as an isotropic phase in thin section light microscopy, is most likely a result of weathering. Rutile as the source of relatively high amounts of Ti was microscopically observed as numerous small aggregates, like leucoxene. Quartz grains (~2 wt.%) were found with a granoblastic texture as a result of rock recrystallization during metamorphism.

The nematogranoblastic texture of meta-gabbro amphibolite (Pit Y-05-07) is mostly composed of hornblende (42.1 wt.%) and plagioclase (12.3 wt.%). The significant proportion of quartz (17.3 wt.%) affecting the content of SiO_2 in bulk chemical composition is a result of replacing some of the melanocratic minerals due to metamorphism of the initial basic rock. Metamorphism also caused the substitution of pyroxenes by amphiboles. Plagioclases are characterized by development of the saussuritization and sericitization. Epidote and chlorite were also found. Supposedly, the X-ray amorphous phase partially corresponds to the weakly anisotropic mass detected in thin section. Traces of muscovite were detected by XRD.

Serpentinous dunite (Pit Y-02-07) illustrates the initial image of the rock. As expected, olivine is the predominant mineral (37.9 wt.%). The content of the serpentine identified as antigorite (26.0 wt.%) reflects the serpentinization of the rock that resulted in the appearance of talc and chlorite as well as traces of amphibole besides serpentine. High sensitivity of the ultrabasic rock to weathering is reflected by reddening of the rock due to the development of Fe-oxides in the micro-cracks in the olivine, serpentine, and chlorite, which are probably reflected by the X-ray amorphous phase.

4.2.2. Porosity (mercury intrusion porosimetry data)

The rocks studied are characterized by similar porosities (8.0–13.8 vol.%), and the highest value was observed for the amphibolite and the lowest for the meta-gabbro amphibolite. Total specific surface area

Table 2
Quantitative mineralogical composition of rock samples determined with Rietveld analysis of XRD-data measured with inner standard zincite and normalized to 100% in wt% with 3σ absolute error.

Components (wt.%)	Amphibolite Pit X-05-3	Meta-gabbro amphibolite Pit Y-05-07	Serpentinous dunite Pit Y-02-07
X-ray amorphous	14.3 ± 2.1	11.1 ± 1.8	11.5 ± 2.4
Olivine	nd	nd	37.9 ± 1.0
Serpentine	nd	nd	26.0 ± 2.7
Talc	nd	nd	3.3 ± 0.8
Chlorite	7.0 ± 1.0	5.3 ± 0.9	13.4 ± 2.2
Amphibole	38.4 ± 2.3	42.1 ± 0.8	5.4 ± 0.5
Epidote	26.7 ± 1.0	7.7 ± 0.5	nd
Plagioclases	9.6 ± 0.6	12.3 ± 0.6	nd
Pyroxenes	1.0 ± 0.4	nd	1.3 ± 0.4
Muscovite	nd	2.4 ± 0.5	nd
Rutile	0.7 ± 0.2	nd	nd
Magnetite	nd	1.8 ± 0.3	0.9 ± 0.3
Quartz	2.3 ± 0.2	17.3 ± 0.4	0.3 ± 0.2

Note: 'nd' — not detected.

Table 3
Porosity characteristics of rock samples, calculated from mercury intrusion porosimetry (MIP).

Rock, Pit	Total cumulative volume (mm³/g)	Total porosity (%)	Total specific surface (m²/g)	Average pore radius[a] (nm)	Pore size distribution: relative volume (mm³/g) and (%) and relative surface (m²/g)		
					58000–1000 (nm)	1000–50	50–1,8
Amphibolite, Pit X-05-3	52.0	13.8	3.0	394.2	2.0 (3.8%) 0.2	48.0 (92.2%) 2.6	2.1 (4.0%) 0.2
Meta-gabbro amphibolite Pit Y-05-07	29.5	8.0	2.5	443.1	9.5 (32.2%) 0.8	17.4 (58.9%) 1.4	2.6 (8.9%) 0.3
Serpentinous dunite Pit Y-02-07	32.0	8.5	3.3	9.0	1.4 (4.5%) 0.2	3.5 (11.1%) 0.4	26.4 (84.4%) 2.7

[a] Average pore radius at 50% of total pore volume.

is also similar (2.5–3.3 m²/g), but there are significant differences in pore size distribution (Table 3, Fig. 3). In serpentinous dunites, more than 90% of the pore volume results from small pores with a radius < 100 nm while the porosity of amphibolite and meta-gabbro amphibolite mainly originates from pores with radii > 100 nm and pores in the size range < 10 nm being almost absent. The amphibolite shows a particularly narrow pore size distribution with approximately 90% of the pores with radii in the range between 100 and 1000 nm (Fig. 3a). The average pore radius is significantly lower in ultrabasic rock compared to basic rock.

4.2.3. Connectivity of pores (Wood's metal data)

In back-scattered electron images of polished sections of the stones, connective pores impregnated with the alloy are visible as the bright phases (Fig. 4). Strong heterogeneity of the connective pores in amphibolite (Pit X-05-3) can be seen in an overview image at low magnification

(×300) based on two types of areas (Fig. 4a): (i) dark sections without any signs of the intruded alloy that indicate that porosity is missing or pore size is below the critical diameter for intrusion (~20 nm) and (ii) sections with almost homogeneously distributed porosity. Here, pores appear well-connected, a good prerequisite for the transport of compounds in pore solution inside the stone. At higher magnification (×1100 and 5000) (Fig. 4b,c), layer silicates in the pores can be clearly identified by their shape. The presence of layer silicates in the pores is important as transport in pores by advection and diffusion might be slowed down due to a narrowing of pore space.

Additionally, pores appear well connected in meta-gabbro amphibolite (Pit Y-05-07) (Fig. 4d). Dark gray areas in the polished section without porosity probably represent quartz. An extended crack system in the sample is observed at high magnification (×1000) (Fig. 4e). From the shape of the connective pores, a strong tortuosity of the pore system can be assumed. In complete contrast amphibolite, phyllosilicates in
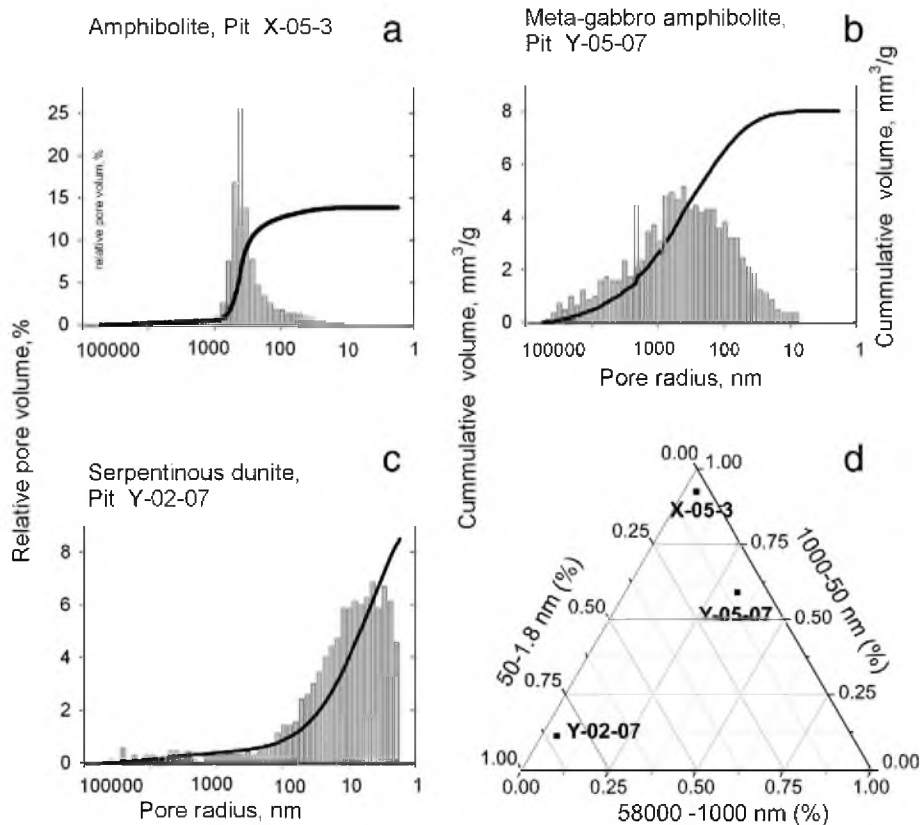

Fig. 3. Pore size distribution of rock samples from amphibolite (a); meta-gabbro amphibolite (b); and serpentinous dunite (c) determined by mercury intrusion porosimetry (MIP) and ternary plot of pore size distribution (custom range) (d).

the pores of meta-gabbro amphibolite are missing, indicating that the chemical weathering rate was generally too low for the formation of secondary phases (Fig. 4f).

In serpentinous dunite (Pit Y-02-07) with a high proportion of phyllosilicates, the connective pore system clearly follows the interspaces of the layer silicates. At low magnification ($\times$100), pore distribution appears homogeneous (Fig. 4g). Zones of phyllosilicate accumulation were observed in regions with higher porosity ($\times$1400) (Fig. 4h). In fractures in the olivine, some fine-dispersed material is also found in the pores besides the layer silicates ($\times$3000) (Fig. 4i).

4.2.4. Topographical microstructure (scanning atomic-force microscopy data)

The topographical microstructures in amphibolite are well-developed and multi-branched with elongated, deep pores (arrow in Fig. 5a) and a net of irregular and shallow pores (DM in Fig. 5a) and initial netlike structures (IM in Fig. 5a). Most likely, the shallow pores could be integrated into a multi-branched net during the process of weathering. In meta-gabbro amphibolite, however, single, elongated deep pores, which might be a grain boundary, begin from funnel-shaped deep pores (squares in Fig. 5b). The intermediate pore surface is smooth. Serpentinous dunite differs significantly from the basic rocks due to the presence of mainly elongated and deep pores with slight roughness of the intermediate pore space (squares in Fig. 5c). The porosity system is characterized by a microstructure of relatively shallow pores with different lengths, depths, and widths.

The microstructures of the basic rocks are similar based on statistical parameters (mean value and root mean square (RMS) value of the height irregularities as well as the "topography" evaluated by the watershed algorithm) and differ from ultrabasic rock (Table 4). The relatively low fractality of meta-gabbro amphibolite suggests the nonfractal nature of the rock, which excludes it from consideration by this approach. However, amphibolite and serpentinous dunite are almost similar according to fractal algorithms.

5. Discussion

The clay mineralogy of the soils from these rocks was the object of our former research (Lessovaia and Polekhovsky, 2009; Lessovaia et al., 2012): (i) only an insignificant accumulation of phyllosilicates was detected in soil from amphibolite, which illustrates the weak pedogenic alteration of the inherited minerals; (ii) soil from meta-gabbro amphibolite is enriched by chlorite and illite as well as the products of their transformation; and (iii) two smectites (saponite and nontronite) and vermiculite in addition to serpentine, talc, and chlorite inherited from the rock represent the mineral association in the <1 μm fraction of soils from the ultrabasic rock. Thus based on the rock characteristics and soil mineralogy of both mature profiles (Pit Y-05-07 and Pit Y-02-07), the increase in SiO_2 in the upper part of the soil from meta-gabbro amphibolite is most likely due to the residual accumulation of inherited quartz whereas soil from ultrabasic rock is assigned by the allochthonous material.
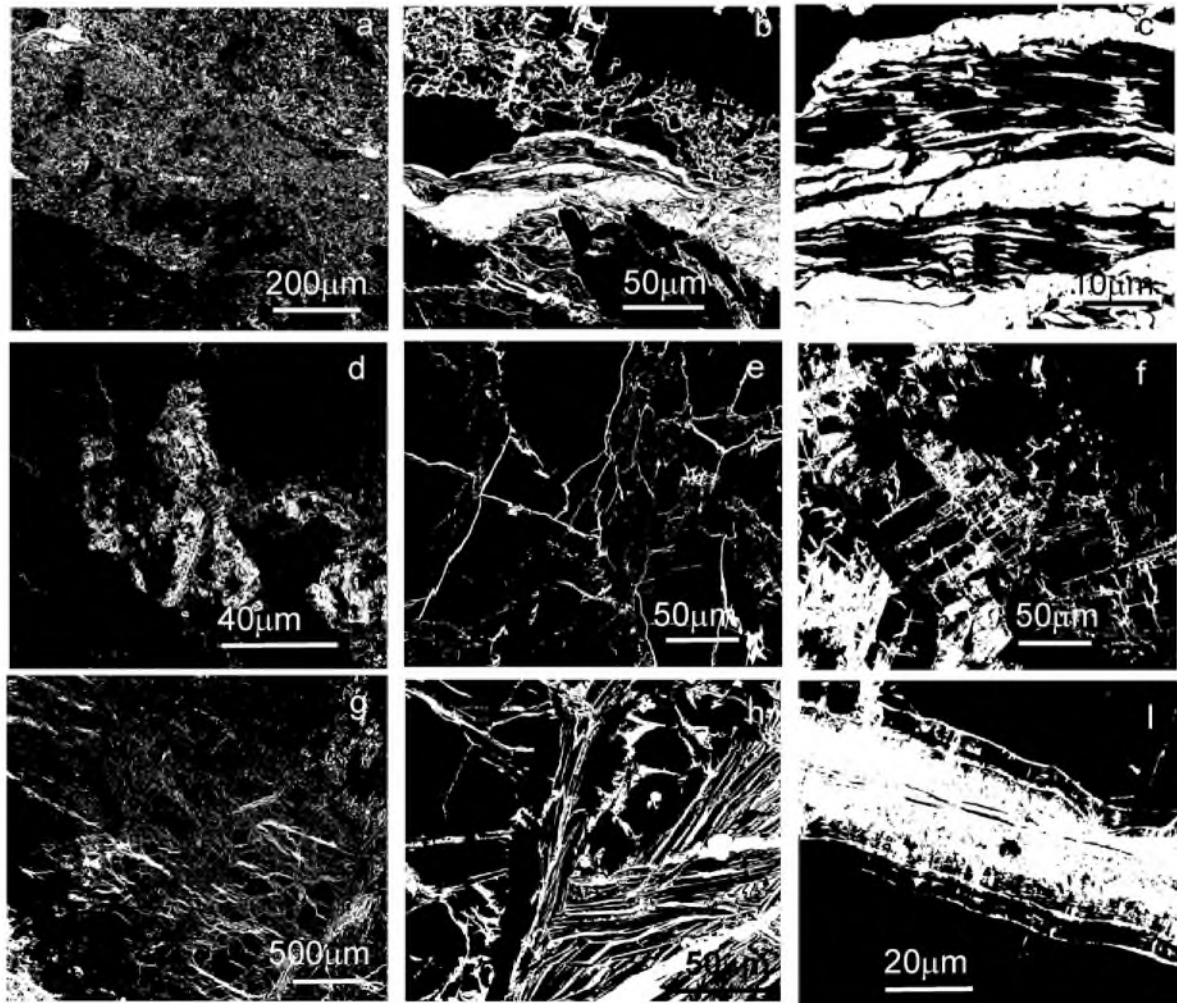

Fig. 4. Back scattered electron images of pore networks in polished sections of rock samples. The connective pore system appears white in the images due to the intrusion of the molten alloy "Wood's metal". Detail images from samples of amphibolite (a, b, c), meta-gabbro amphibolite (d, e, f), and serpentinous dunite (g, h, i).
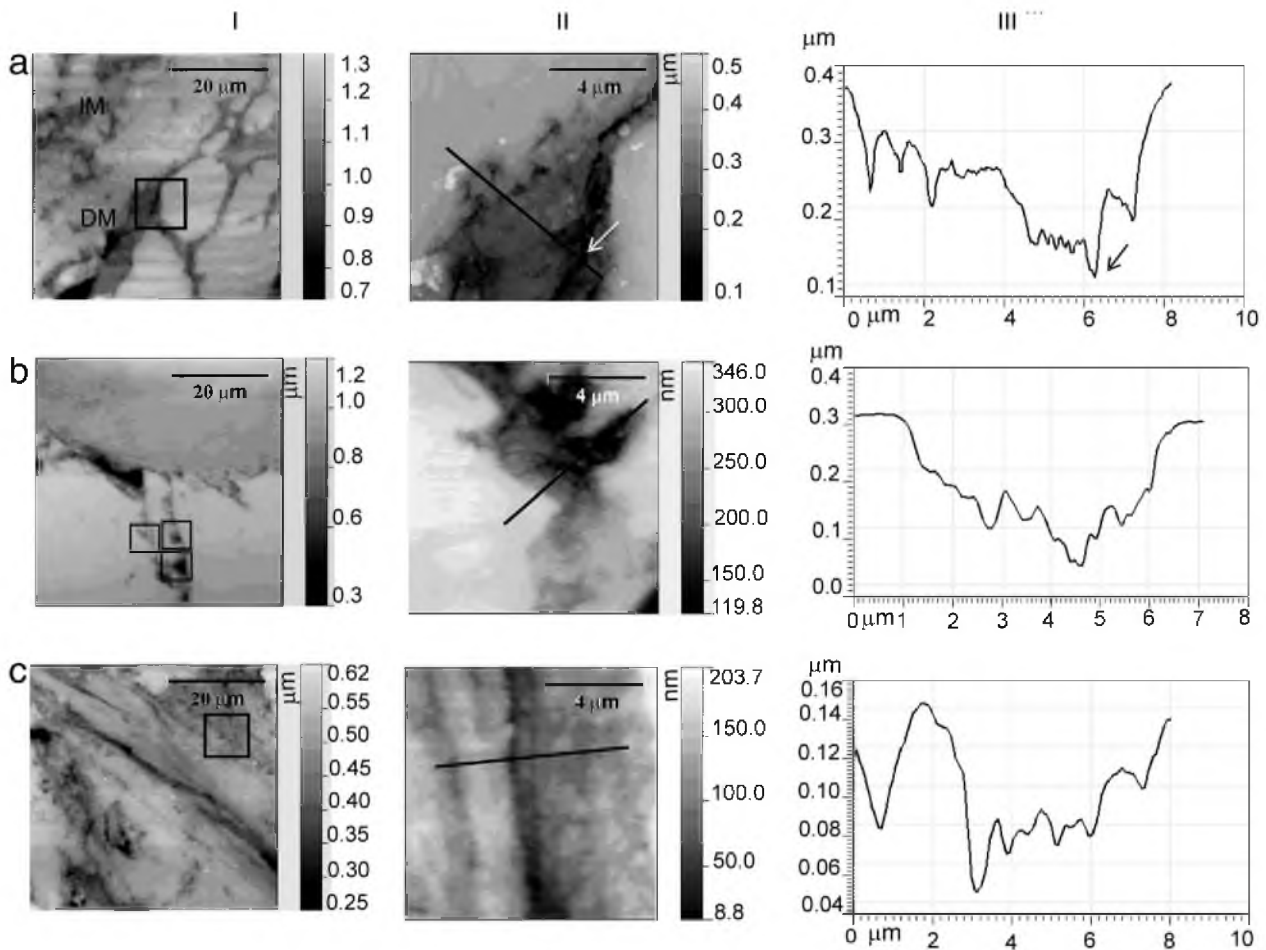
Fig. 5. Topography of open spaces in the polished surface of sections of the rock samplers determined by atomic-force microscopy: amphibolite (a), meta-gabbro amphibolite (b), and serpentinous dunite (c). Overview image (50 × 50 μm) (I) and detail image (10 × 10 μm) (II) with the gray scales to associate the color with the height of the relief (on the right side of each image); the position of the topographic profile and cross sectional view of the topographic profile (III). IM — initial netlike and DM well-developed multi-branched porosity system.

Serpentinous dunite is, based on its mineralogical composition and porosity, the most weatherable of the rocks under consideration, which explains the appearance of smectites in the soil that is absent in the rock. Oxidation weathering of olivine that predominated in the studied rock can result in iddingsite, in which rims trioctahedral smectite (saponite) and goethite (αFeOOH) have been reported (Eggleton, 1984; Smith et al., 1987; Wilson, 2004). Weathering of serpentinous dunite can also lead to replacement of the serpentine by smectites as well as chlorite by trioctahedral vermiculite (Caillaud et al., 2006). Intensive chemical weathering is confirmed by reddening of the rock fragments due to the ready oxidation of released Fe (Alexander and DuShey, 2011) and the large amount of dithionite extractable Fe caused by weathering of the fine-grained parent rocks (Hseu et al., 2007).

Additionally, the studied rock is characterized by a porosity system developed with a predominance of small pores and a rough surface. The creation of new voids is most likely a prerequisite for further chemical weathering because the altered products never completely replace the dissolved volume (Putnis, 2002), which could be relics of previous fluid–rock interactions (Navarre-Sitchler et al., 2009), and increase secondary porosity. Thus, the formation of Haplic Cryosol (Reductaquic) (Pit Y-02-07) affected by acidification and gleization has been taking place in the "mature" fine earth enriched by smectites that are absent in the rock.

Lower sensitivity to weathering of the basic rocks is correlated with a predominance of large pores and the near absence of pores with radii < 10 nm in size, which can be attributed to the presence of layer

Table 4
Statistical parameters of sample microstructure calculated from data obtained by scanning atomic-force microscopy on polished sections from rock samples.

Rock parameter	Mean value	RMS value	Evaluation of sample "topography" by watershed algorithm[a] (%)	Fractal dimension by algorithm	
	Height irregularities (μm)			Cube counting	Binary decomposition of image intensity field
Amphibolite Pit X-05-3	1.102	0.110	30	2.22	2.52
Meta-gabbro amphibolite Pit Y-05-07	0.995	0.107	15–20	2.11	2.23
Serpentinous dunite Pit Y-02-07	0.517	0.075	≥50	2.21	2.46

Note: RMS — root mean square.
[a] Proportion of the total projected area of pores related to whole scanned area.

silicates based on the example of altered mid-ocean ridge basalts (Simonyan et al., 2012). Relatively high amphibole content in both types of basic rocks can result in the crystallization of smectites caused by weathering (Proust et al., 2006; Wilson and Farmer, 1970) or neoformed kaolinite as well as goethite and gibbsite that result from precipitation from the solution of ferruginous and aluminous weathering products (Velbel, 1989). However, insignificant proportions of phyllosilicates in both types of the basic rocks studied (Table 2) demonstrate the low intensity of chemical weathering.

Supposedly, a particularly narrow distribution of pore size with predominantly large pores in amphibole is a reason for the insignificant accumulation of phyllosilicates in shallow Lithic Leptosol (Pit X-05-3) despite the detection of the rare zones with phyllosilicate accumulation and a well-developed multi-branched microstructure, which is similar to that in serpentinous dunite based on the fractal dimension algorithm (Table 4). Thus, pedogenesis leads to the formation of fine earth predominantly through rock disintegration.

Unlike Lithic Leptosol, Epileptic Entic Podzol on meta-gabbro amphibolite are enriched by phyllosilicates that correlate with the presence of pores with radii below 10 nm that are connected with layer silicates (Simonyan et al., 2012). However, the predominantly smooth surface of the inter-pore space, as well as the absence of phyllosilicate accumulation along the pores and the empty space inside the pores, indicates the limitation of tracing the potential source of phyllosilicates by weathering. It is more likely that rock desegregation and weathering, which is confirmed by the relatively high proportion of soluble Al in the bottom horizons, were enough to provide sufficient amounts of clay minerals to the soil.

6. Conclusions

The present research illustrates that the difference between the rocks types including details of the porosity system gives rise to secondary mineral products and is a significant factor in tracing the mineralogy of soil clay in soils formed from hard rocks. The sensitivity of ultrabasic rock to weathering is affected by (i) the high number of small pores, especially with radii < 10 nm in size; (ii) the elongated form of the pores and surface roughness; and (iii) the zones with phyllosilicate accumulation in regions with higher porosity. Pedogenesis from the rock demonstrates the possibility of soil formation from the "mature" fine earth enriched by smectites absent in the rock. Thus, serpentinous dunite, with dominantly interlinked fine pores, is a suitable substrate for the appearance of secondary minerals (smectites).

Despite the presence of low proportions of phyllosilicates in both types of the basic rocks studied, only soil from meta-gabbro amphibolite is enriched by clay minerals, which is most probably affected by the presence of the smallest pores with radii <10 nm in size. The absence of phyllosilicate accumulation along the pores and the predominantly empty space inside the pores indicates the limitation of potential sources of phyllosilicates for developing soil from meta-gabbro amphibolite. Insignificant accumulation of phyllosilicates in the shallow soil from amphibolite, in which the fine size fractions are mostly the result of rock disintegration, is supposedly due to a particularly narrow pore size distribution with a predominance of pores between 100 and 1000 nm. Thus, metagabbro amphibolite, with more small pores, is more likely to give rise to clay minerals than the amphibolite, with a narrow distribution of larger pores, although even the former shows little tendency for clay minerals to accumulate within pores.

Acknowledgments

References

Alexander, E.B., DuShey, J., 2011. Topographic and soil differences from peridotite to serpentinite. Geomorphology 135, 271–276.
Allen, Ch.E., 2002. The influence of schistocity on soil weathering on large boulder tops, Kärkevagge, Sweden. Catena 49, 157–169.
Arnaud, R.J.S.T., Whiteside, E.P., 1963. Physical breakdown in relation to soil development. Eur. J. Soil Sci. 14, 267–281.
Bergmann, J., Kleeberg, R., 1998. Rietveld analysis of disordered layer silicates. Mater. Sci. Forum 278–281, 300–305.
Bergmann, J., Friedel, P., Kleeberg, R., 1998. BGMN — a new fundamental parameters based Rietveld program for laboratory X-ray sources, it's use in quantitative analysis and structure investigations. CPD Newsletter 20. Commission of Powder Diffraction, International Union of Crystallography, pp. 5–8.
Bish, D.L., Plötze, M., 2011. X-ray powder diffraction with emphasis on qualitative and quantitative analysis in industrial mineralogy. In: Christidis, G. (Ed.), Industrial Mineralogy, EMU Notes in Mineralogy vol. 9, pp. 35–76 (Chapter 3).
Borden, P.W., Ping, C.-Lu., McCarthy, P.J., Naidu, S., 2010. Clay mineralogy in arctic tundra gelisols, northern Alaska. Soil Sci. Soc. Am. J. 74 (2), 580–592.
Caillaud, J., Proust, D., Righi, D., 2006. Weathering sequences of rock-forming minerals in a serpentinite: influence of microsystems on clay mineralogy. Clays Clay Minerals 54 (1), 87–100.
Chernyakhovskii, A.G., 1994. Eluvial process and soil formation (Eluvial'nyi prozess e pochvoobrazovanie). Nauka, Moscow (in Russian).
Darot, M., Reuschle, T., 1999. Direct assessment of Wood's metal wettability on quartz. Pure Appl. Geophys. 155, 119–129.
Dultz, S., Behrens, H., Simonyan, A., Kahr, G., Rath, T., 2006. Determination of porosity and pore connectivity in feldspars from soils of granite and saprolite. Soil Sci. 171, 675–694.
Eggleton, R.A., 1984. Formation of iddingsite rims on olivine: a transmission electron microscope study. Clays Clay Minerals 32, 1–11.
Hseu, Z.Y., Tsai, H., Hsi, H.C., Chen, Y.C., 2007. Weathering sequences of clay minerals in soils along a serpentinitic toposequence. Clays Clay Minerals 55, 389–401.
Jackson, M.L., Lim, C.H., Zelazny, L.W., 1986. Oxides, hydroxides, and aluminosilicates. In: Klute, A. (Ed.), Methods of Soil Analysis. Part 1, 2nd ed., pp. 101–150.
Kaufmann, J., 2009. Characterization of pore space of cement-based materials by combined mercury and Wood's Metal intrusion. J. Am. Ceram. Soc. 92, 209–216.
Klapetek, P., Ohlidal, I., Franta, D., Montaigne-Ramil, A., Bonanni, A., Stifter, D., Sitter, H., 2003. Atomic force microscopy characterization of ZnTe epitaxial films. Acta Phys. Slovaca 3 (53), 223–230.
Lessovaia, S.N., Polekhovsky, Yu.S., 2009. Mineralogical composition of shallow soils on basic and ultrabasic rocks of East Fennoscandia and of the Ural Mountains, Russia. Clays Clay Minerals 57, 476–485.
Lessovaia, S., Dultz, S., Polekhovsky, Yu., Krupskaya, V., Vigasina, M., Melchakova, L., 2012. Rock control of pedogenic clay mineral formation in a shallow soil from serpentinous dunite in the Polar Urals, Russia. Appl. Clay Sci. 64, 4–11.
Lessovaia, S.N., Goryachkin, S.V., Desyatkin, R.V., Okoneshnikova, M.V., 2013. Pedoweathering and mineralogical change in Cryosols in an ultracontinental climate (Central Yakutia, Russia). Acta Geodyn. Geomater. 10 (172), 465–473 (No. 4).
Lloyd, R.R., Provis, J.L., Smeaton, K.J., van Deventer, J.S.J., 2009. Spatial distribution of pores in fly ash-based inorganic polymer gels visualised by Wood's metal intrusion. Microporous Mesoporous Mater. 126, 32–39.
Mehra, O.P., Jackson, M.L., 1958. Iron oxide removal from soils and clays by a dithionite–citrate system buffered with sodium bicarbonate. Clays Clay Minerals 7, 317–327.
Navarre-Sitchler, A., Steefel, C.I., Yang, L., Tomutsa, L., Brantley, S.L., 2009. Evolution of porosity and diffusivity associated with chemical weathering of a basalt clast. J. Geophys. Res. 114, 14. http://dx.doi.org/10.1029/2008JF001060 art. no. F02016.
Proust, D., Caillaud, J., Fontaine, C., 2006. Clay minerals in early amphibole weathering: tri- to dioctahedral sequence as a function of crystallization sites in the amphibole. Clays Clay Minerals 54, 351–362.
Putnis, A., 2002. Mineral replacement reactions: from macroscopic observations to microscopic mechanisms. Mineral. Mag. 66, 689–708.
Schuessler, J.A., Botcharnikov, R.E., Behrens, H., Misiti, V., Freda, C., 2008. Oxidation state of iron in hydrous phono-tephritic melts. Am. Mineral. 93, 1493–1504.
Sedov, S.N., Vaseneva, E.G., Shoba, S.A., 1992. Modern and ancient processes of weathering in soils from basic rocks in Valaam Island (Sovremennye e drevnie prozessy vyvetrivaniya v pochvakh na osnovnykh porodakh ostrova Valaam). Pochvovedenie 7, 83–96 (in Russian).
Simas, F.N.B., Schaefer, C.E.G.R., Melo, V.F., Guerra, M.B.B., Saunders, M., Gilkes, R.J., 2006. Clay sized minerals in permafrost-affected soils (Cryosols) from King George Island, Antarctica. Clays Clay Minerals 54, 721–736.
Simonyan, A.V., Dultz, S., Behrens, H., 2012. Diffusive transport of water in porous fresh to altered mid-ocean ridge basalts. Chem. Geol. 306–307, 63–77.
Smith, K., Milnes, A., Eggleton, R.A., 1987. Weathering of basalt: formation of iddingsite. Clays Clay Minerals 35 (6), 418–428.
Tyurin, E.V., 1931. New modification of volume method for determination of humus by chromic acid (Novoe vidoizmenenie ob'emnogo metoda opredeleniya gumusa s pomosh'u khromovoi kisloty). Pochvovedenie 37, 515–524 (in Russian).
Velbel, M.A., 1989. Weathering of hornblende to ferruginous products by a dissolution–reprecipitation mechanism: petrography and stoichiometry. Clays Clay Minerals 37, 515–524.
Velde, B., Meunier, A., 2008. The Origin of Clay Minerals in Soils and Weathered Rocks. Springer-Verlag, Berlin, Heidelberg, New York.
Washburn, E.W., 1921. Note on a method of determining the distribution of pore sizes in a porous material. Proc. Natl. Acad. Sci. U. S. A. 7, 115–116.

Whitney, D.L., Evans, B.W., 2010. Abbreviations for names of rock-forming minerals. Am. Mineral. 95, 185–187.

Wilson, M.J., 2004. Weathering of the primary rock-forming minerals: processes, products and rates. Clay Miner. 39, 233–266.

Wilson, M.J., Farmer, V.C., 1970. A study of weathering in a soil derived from a biotite–hornblende rock II. The weathering of hornblende. Clay Miner. 8, 435–444.

World Reference Base for Soil Resources, 2006. World Soil Resources Reports 103. 2nd edition. FAO, Rome.